NRL Report 8465

Multifocal Three Dimensional Bootlace Lenses

JAGANMOHAN B. L. RAO

Search Radar Branch
Radar Division

March 12, 1981

NAVAL RESEARCH LABORATORY
Washington, D.C.

SECURITY CLASSIFICATION OF THIS PAGE *(When Data Entered)*

REPORT DOCUMENTATION PAGE		READ INSTRUCTIONS BEFORE COMPLETING FORM
1. REPORT NUMBER NRL Report 8465	2. GOVT ACCESSION NO.	3. RECIPIENT'S CATALOG NUMBER
4. TITLE *(and Subtitle)* MULTIFOCAL THREE DIMENSIONAL BOOTLACE LENSES		5. TYPE OF REPORT & PERIOD COVERED Final report on one phase of a continuing project. 6. PERFORMING ORG. REPORT NUMBER
7. AUTHOR(s) Jaganmohan B. L. Rao		8. CONTRACT OR GRANT NUMBER(s)
9. PERFORMING ORGANIZATION NAME AND ADDRESS Naval Research Laboratory Washington, DC 20375		10. PROGRAM ELEMENT, PROJECT, TASK AREA & WORK UNIT NUMBERS 63516N; S0168-AA; 0640-0
11. CONTROLLING OFFICE NAME AND ADDRESS Department of the Navy Naval Sea Systems Command Washington, DC 20362		12. REPORT DATE March 12, 1981 13. NUMBER OF PAGES 27
14. MONITORING AGENCY NAME & ADDRESS*(if different from Controlling Office)*		15. SECURITY CLASS. *(of this report)* UNCLASSIFIED 15a. DECLASSIFICATION/DOWNGRADING SCHEDULE

16. DISTRIBUTION STATEMENT *(of this Report)*

Approved for public release; distribution unlimited.

17. DISTRIBUTION STATEMENT *(of the abstract entered in Block 20, if different from Report)*

18. SUPPLEMENTARY NOTES

19. KEY WORDS *(Continue on reverse side if necessary and identify by block number)*

Multifocal	Bifocal
Bootlance lenses	Trifocal
Three dimensional	Quadrufocal
Multiple beam antennas	

20. ABSTRACT *(Continue on reverse side if necessary and identify by block number)*

It is well known that a two dimensional (parallel plate configuration) bootlace lens can be designed to have more than one focal point. Wide angle scanning capabilities of these lenses in two dimensions is well established, being larger for higher number of focal points. However, no three dimensional bootlace lens having more than one focal point has been reported. It is the purpose here to report on three dimensional bootlace lenses having two, three and four perfect focal points. Equations for lens surfaces are obtained for all three cases. An analysis shows that a lens with a larger number of focal points can be scanned to much

(Continued)

DD FORM 1 JAN 73 1473 EDITION OF 1 NOV 65 IS OBSOLETE
S/N 0102-LF-014-6601

SECURITY CLASSIFICATION OF THIS PAGE *(When Data Entered)*

20. ABSTRACT (Continued)

larger angles in one plane at the expense of a modest decrease in scanning capability in the orthoganal plane. Computer simulations of radiation patterns for different scan angles are presented for all three lenses. These results also show that a lens with a higher number of focal points can be scanned to larger angles.

CONTENTS

MULTIFOCAL THREE DIMENSIONAL BOOTLACE LENSES

INTRODUCTION

It is well known that a two dimensional (parallel plate configuration) bootlace lens can be designed to have more than one focal point [1-3]. Wide angle scanning capabilities of these lenses in two dimensions is well established, being larger for higher numbers of focal points. Similarly, Ruze [4] has demonstrated the wide-angle scanning capability of cylindrical metal plate lenses designed to have two focal lines. Dion and Ricardi [5] reported on a three dimensional waveguide lens which has two perfect focal points. The spherical-planar lens [6] is a three dimensional bootlace lens having a single focal point. However, no three dimensional bootlace lens having more than one focal point has been reported. It is the purpose here to report on three dimensional bootlace lenses having two, three and four focal points. Equations for lens surfaces are obtained first for all three cases. An analysis is included on aperture phase errors, which shows that the scanning capability of a lens, in the scan plane, will increase as the number of focal points is increased. Computer simulation of radiation patterns for different scan angles confirmed this.

BIFOCAL THREE DIMENSIONAL BOOTLACE LENS

Figure 1 shows the cross section of a bifocal lens in the XZ-plane which is also the scan plane. The points S_1 and S_2 are two conjugate foci which lie on a straight line, parallel to the X-axis, in the XZ plane. The feed side of the lens has a curved surface, where the pickup elements are placed. The other side of the lens is a planar surface, where the radiating elements are placed. Flexible transmission lines of length L are used in connecting pickup elements to the corresponding radiation elements. The line S_1C makes an angle α with the negative Z-axis. It is required that the main beam lie in UW-plane and is directed at an angle $-\alpha$ to the W-axis when the feed is placed at S_1, and α to the W-axis when the feed is at S_2.

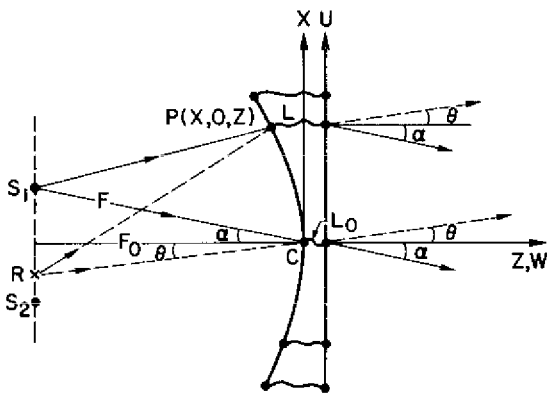

Fig. 1 — Bifocal lens geometry in XZ-plane

Manuscript submitted on December 2, 1980.

Lens surfaces are obtained by using the following procedure. The lens cross section in the XZ-plane is obtained first by treating the problem as if it is a two dimensional case with the specified number of focal points. Then, the inner lens surface is obtained by rotating the inner lens cross section with the feed line (straight line passing through the focal points) as the axis of rotation. The outer surface is obtained by simply extending the outer cross section of the lens in positive and negative directions of the V-axis. If S_1 and S_2 are two focal points for the lens cross section in XZ-plane, it is not difficult to verify that they are also perfect focal points for the three dimensional lens obtained by using the above procedure. The same procedure is applied later, to trifocal and quadrufocal lenses.

In what follows, the lens parameters are determined by using the fact that the path length from the focal point to any point on the corresponding wave front is a constant. Applying this condition to the two rays emanating from S_1 in Fig. 1, we have

$$\overline{S_1P} + L + U \sin\alpha = F + L_o, \tag{1}$$

where L, L_o are the transmission line lengths at a general point P and the origin C respectively, $F = S_1C$, and

$$\overline{S_1P} = \sqrt{(X - F\sin\alpha)^2 + (Z + F\cos\alpha)^2}. \tag{2}$$

Similarly, applying path length equality between a general ray and the ray passing through the origin, which emanates from S_2, one obtains

$$\overline{S_2P} + L - U \sin\alpha = F + L_o, \tag{3}$$

where

$$S_2P = \sqrt{(X + F\sin\alpha)^2 + (Z + F\cos\alpha)^2}. \tag{4}$$

The following relation can be obtained using equations (1) and (3):

$$\overline{S_1P}^2 - \overline{S_2P}^2 = -4\,U\sin\alpha\,(F + L_o - L). \tag{5}$$

From Eqs. (2) and (4), one obtains

$$\overline{S_1P}^2 - \overline{S_2P}^2 = -4\,FX\sin\alpha. \tag{6}$$

Since the left hand side terms of Eqs. (5) and (6) are equal, the right hand side terms should be equal. This will be satisfied if the transmission line lengths are equal, and the X-coordinate of a pickup element is equal to the U-coordinate of the corresponding radiating element. Therefore we obtain

$$L = L_o \text{ and } X = U. \tag{7}$$

Eliminating L and U from (1) using (7) and substituting $\overline{S_1P}$ from (1) in (2) gives the inner lens cross section in the XZ-plane and is given by

$$(F - X\sin\alpha)^2 = F^2 + X^2 + Z^2 + 2\,FZ\cos\alpha - 2\,FX\sin\alpha. \tag{8}$$

Rearranging the terms in Eq. (8), we have

$$Z^2 + X^2\cos^2\alpha + 2\,FZ\cos\alpha = 0. \tag{9}$$

As discussed earlier, the inner lens surface can be obtained by rotating the cross secton given by Eq. (9) about the feed line (line passing through the two foci). Therefore, the equation for the inner lens surface is given by

$$Z^2 + X^2\cos^2\alpha + Y^2 + 2\,FZ\cos\alpha = 0. \tag{10}$$

The corresponding V coordinate of the radiating element can be obtained from $V = Y$ and U-coordinate is given by (7).

Equation (10) is the mathematical expression of a spheroid whose trace in the XZ-plane is given by Eq. (9), which can be rewritten as

$$\frac{X^2}{F^2} + \frac{(Z + F\cos\alpha)^2}{F^2\cos^2\alpha} = 1, \tag{11}$$

i.e., an ellipse with foci at the two focal points S_1 and S_2, and the trace of Eq. (10) in the YZ-plane is

$$Y^2 + (Z + F\cos\alpha)^2 = F^2\cos^2\alpha, \tag{12}$$

i.e., a circle of radius $F_o = F\cos\alpha$.

It is noted that the Eqs. (10), (11), and (12), representing the contour of the inner surface of the lens, are the same as Eqs. (3), (4) and (5) of Dion and Ricardi [5]. However, for the lens being discussed here, the outer surface is planar and the path lengths between the surfaces is a constant, whereas, for the waveguide lens discussed by Dion and Ricardi [5], the outer surface is an ellipsoid (given by their Eq. (6)) and the path lengths between two surfaces are unequal.

The bifocal lens is symmetrical with respect to the YZ-plane and axially asymmetric. It may be noted that, if the two foci are allowed to merge together on the axis of the lens, the angle α becomes zero. Under this condition the lens becomes axially symmetric with the surface facing the feed becoming a segment of a sphere centered at the feed while the opposite surface is still planar. This limiting case corresponds to the geometry of a spherical-planar lens discussed by Patton [6], which is a single focus lens. As an example, Fig. 2 shows the bifocal lens cross section in the XZ-plane for $\alpha = 10°$.

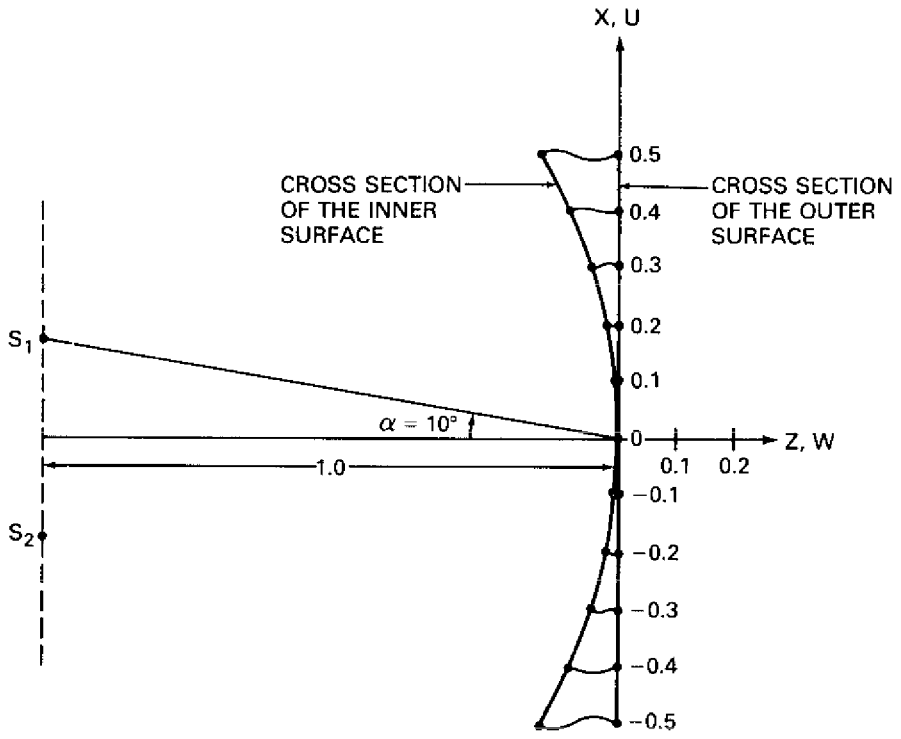

Fig. 2 — Cross section of a bifocal lens in XZ-plane, $\alpha = 10°$

APERTURE PHASE ERRORS: BIFOCAL LENS

When a feed is placed at one of the focal points, the emitted phase-front corresponds to a constant path-length (no phase errors). However, when the feed is displaced from those focal points to scan the beam to other angles, the corresponding wavefront will have some phase errors. If the feed displacement is confined to the line passing through the two focal points, the phase errors will be independent of the Y-coordinate (hence V-coordinate) and depends only on the X-coordinate (or U-coordinate) and the scan angle θ. Therefore, to know the aperture phase errors, one needs to find only the phase errors on the aperture cross section in the UW plane. It is the purpose of this section to study these errors for a bifocal lens and compare the results with that of a single focus lens. For this purpose, the feed is assumed to be located at an arbitrary point R on a line which is parallel to the X-axis and passes through the focal points, as shown in Fig. 1.

Let the line $\overline{RC}$ make an angle θ with the negative Z-axis. Then, the main beam direction should be at an angle θ from the W-axis, as shown in Fig. 1. The coordinates of the feed point R are given by $(-F\cos\alpha\tan\theta,\ 0,\ -F\cos\alpha)$.

The path-length from the feed position R to the wavefront, for a ray passing through a point $P(X,\ Z)$, is given by

$$L_p = \overline{RP} + L_o - U\sin\theta, \tag{13}$$

and for the ray passing through the origin C, it is given by

$$L_c = \overline{RC} + L_o. \tag{14}$$

The path-length error is given by

$$\Delta L = L_p - L_c = \overline{RP} - \overline{RC} - U\sin\theta. \tag{15}$$

From Fig. 1, one can obtain the values of $\overline{RP}$ and $\overline{RC}$ as

$$\overline{RP} = \sqrt{(X + F\cos\alpha\tan\theta)^2 + (Z + F\cos\alpha)^2} \tag{16}$$

and

$$\overline{RC} = F\cos\alpha/\cos\theta. \tag{17}$$

Eliminating Z from (16) using (9) and then substituting $\overline{RP}$ and $\overline{RC}$ values in (15), the normalized path length error is given by

$$\frac{\Delta L}{F_o} = -u\sin\theta - \frac{1}{\cos\theta} + \sqrt{\frac{1}{\cos^2\theta} + u^2\sin^2\alpha + 2u\tan\theta}, \tag{18}$$

where $u = U/F_o$ and $F_o = F\cos\alpha$.

For comparison, the path-length error for a single focus lens can be obtained from (18) by assuming $\alpha = 0$ and is given by

$$\frac{\Delta L_o}{F_o} = -u\sin\theta - \frac{1}{\cos\theta} + \sqrt{\frac{1}{\cos^2\theta} + 2u\tan\theta}. \tag{19}$$

Figure 3 shows normalized path length errors for a bifocal ($\alpha = 10°$) and the single focus lens as a function of normalized aperture u. From Fig. 3, it may be noted that, when the normalized aperture is limited to ± 0.5, the maximum error occurs at $u = -0.5$ for any given scan angle θ. Figure 4 shows this maximum path error on the aperture ($u = -0.5$) vs scan angle. For single focus lens, the magnitude of the path-length error increases as the scan angle is increased. For bifocal lens, the path error

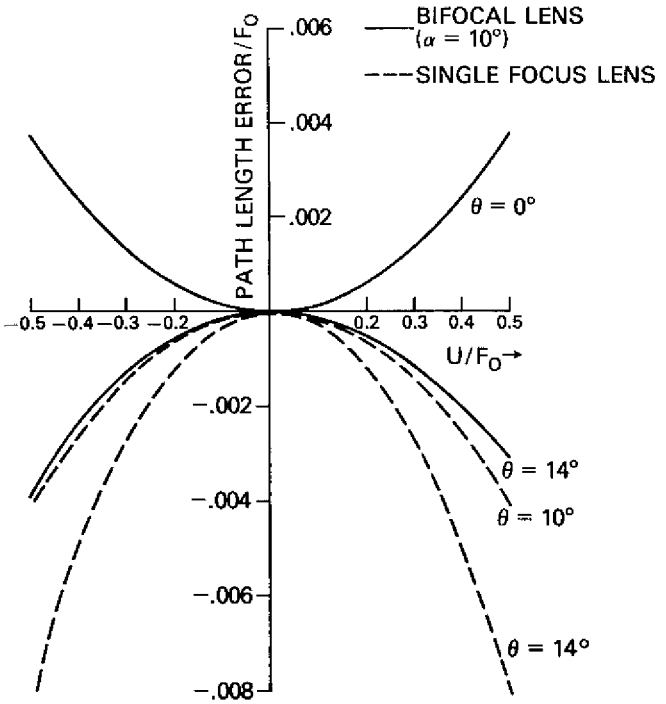

Fig. 3 — Path length errors in *XZ*-plane

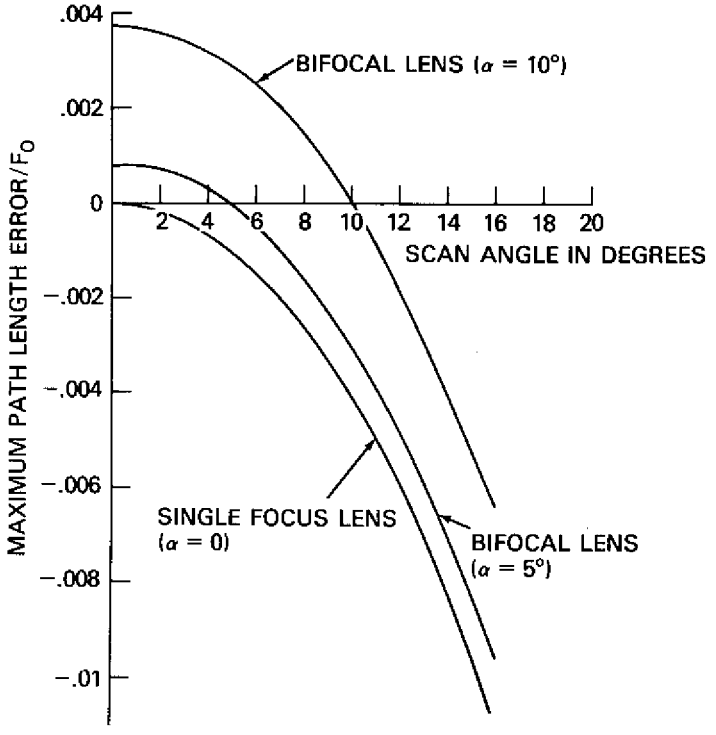

Fig. 4 — Path length error vs scan angle (for $u = -0.5$)

will be maximum for zero scan angle and decreases monotonically with the increase in scan angle, reaching zero error at the scan angle α. Then, the magnitude of the path error increases monotonically for scan angles greater than α. From Fig. 4 it may be noted that for $\alpha = 10°$, the bifocal lens will have normalized path errors less than .004 over a scanning range of $\pm 14°$, whereas the single focus lens can only be scanned to slightly less than $\pm 10°$. Therefore, some 40% more scanning range is possible with bifocal lens compared to a single focus lens. Similar conclusion can be reached for the case of $\alpha = 5°$, shown in Fig. 4. As noted before, for scan angles less than α, maximum path error occurs at zero scan angle. Figure 5 shows this maximum path error vs α. This curve will be useful in choosing α for a specified maximum phase (or path length) error with the understanding that the maximum scan angle is approximately equal to $\pm 1.4\ \alpha$ for the specified phase error.

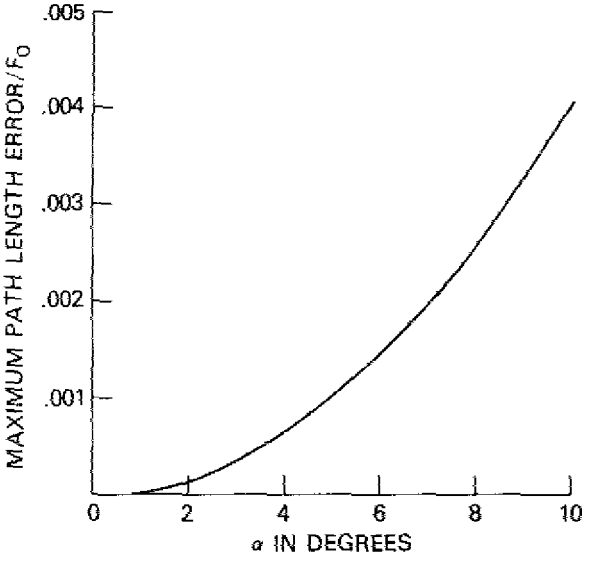

Fig. 5 — Peak path length error vs α for bifocal lens with $(F_0/D) = 1$

TRIFOCAL THREE DIMENSIONAL BOOTLACE LENS

It was shown that a three dimensional bootlace lens having two perfect focal points can be used as a multiple beam antenna or can be used to scan more beamwidths compared to a lens having only a single focus. However, its scanning capability is still limited. It will be shown that a three dimensional bootlace lens with three perfect focal points has a wider angle scanning capability compared to a bifocal lens.

The trifocal lens design differs from the bifocal model in that the corresponding points on the two lens contours (X and U components in Fig. 6) are not equidistant from the YZ-plane. This additional degree of freedom in design permits specification of a third focal point. However, to be a perfect focal point in three dimensions, the location of the third focal point should be on a line joining the pair of conjugate foci S_1 and S_2, and symmetry condition dictates it to be on the axis of symmetry, as shown in Fig. 6.

Figure 6 shows the cross section of a trifocal lens in the XZ-plane. The points S_0, S_1, and S_2 are perfect focal points for radiation at angles 0, $-\alpha$, and α to the W-axis, respectively. They are located, in the XZ-plane, on a line parallel to the X-axis. The coordinates of these focal points are given by (0, 0, $-F_0$), ($F \sin \alpha$, 0, $-F \cos \alpha$), and ($-F \sin \alpha$, 0, $-F \cos \alpha$), respectively, relative to the origin C. Considering a central ray passing through the origin C, and a general ray passing through the point

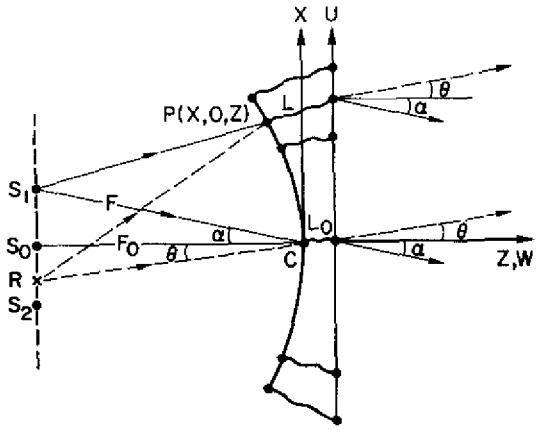

Fig. 6 — Trifocal lens geometry in XZ-plane

$P\ (X,\ Z)$, both originating from focal point S_1, the condition for optical path length equality gives the following relation:

$$\overline{S_1P} + L + U \sin\alpha = F + L_0, \tag{20}$$

where

$$\overline{S_1P} = \sqrt{(X - F\sin\alpha)^2 + (Z + F\cos\alpha)^2}, \tag{21}$$

L = Transmission line length at a general point P,

and L_0 = Transmission line length at the origin C.

Similarly, applying the condition for path length equality of central and general rays originating from the focal points S_2 and S_0, one obtains

$$\overline{S_2P} + L - U \sin\alpha = F + L_0, \tag{22}$$

$$\overline{S_0P} + L = F_0 + L_0, \tag{23}$$

where

$$\overline{S_2P} = \sqrt{(X + F\sin\alpha)^2 + (Z + F\cos\alpha)^2}, \tag{24}$$

and

$$\overline{S_0P} = \sqrt{X^2 + (Z + F_0)^2}. \tag{25}$$

From Eqs. (20) and (22) we have

$$\overline{S_2P}^2 - \overline{S_1P}^2 = 4\ U \sin\alpha (F + L_0 - L), \tag{26}$$

and from Eqs. (21) and (24) we obtain

$$\overline{S_2P}^2 - \overline{S_1P}^2 = 4\ FX \sin\alpha. \tag{27}$$

Excluding the degenerate case of $\alpha = 0$ (in that case S_1 and S_2 merge into a single point on axis; consequently, there will be less than three focal points), and equating the right hand sides of Eqs. (26) and (27) one obtains

$$FX = U\ (F + L_o - L). \tag{28}$$

Equation (28) gives a relation between X, U and $L - L_o$. An equation relating U and $L - L_o$ can be obtained as follows. Substituting the value of $\overline{S_1P}$ from (20) in (21) and eliminating X (but not X^2) using (28), one obtains

$$X^2 + Z^2 + 2\,ZF\cos\alpha = 2\,F\,(L_o - L) + (L_o - L)^2 + U^2\sin^2\alpha. \tag{29}$$

Similarly, substituting $\overline{S_oP}$ from (23) in (25) we get

$$X^2 + Z^2 + 2\,ZF_o = 2\,F_o\,(L_o - L) + (L_o - L)^2. \tag{30}$$

The left hand sides of (29) and (30) are equal because $F_o = F\cos\alpha$. So, equating the right hand sides gives an equation relating U and $L - L_o$ as

$$L - L_o = \frac{U^2}{F}\cos^2(\alpha/2). \tag{31}$$

Equation (30) represents the cross section in the XZ-plane of the inner surface of the trifocal lens with X, U and $L - L_o$ related as shown in (28) and (31).

For specified values of design parameters α, F_o, and the element location U on the radiating surface, Eq. (31) can be used to find the corresponding $L - L_o$. Then, the corresponding value of X can be found by substituting the known values of α, F_o, U, and $L - L_o$ in (28). Finally, the corresponding Z coordinate of the inner lens surface can be found from (30), knowing X, F_o and $L - L_o$. By assuming different values for U, complete inner surface cross section in XZ-plane can be obtained. As an example, Fig. 7 shows the cross section of a trifocal lens for $\alpha = 15°$. The three dimensional inner surface of the lens can be obtained by rotating this cross section about the line on which the focal points are located. This completes the design procedure of the lens.

Requirements on the scanning range, allowable aperture phase errors, and the aperture size will determine what values should be chosen for design parameters α and F_o. In this regard, the analysis on aperture phase errors, which is discussed in the next section, will be useful.

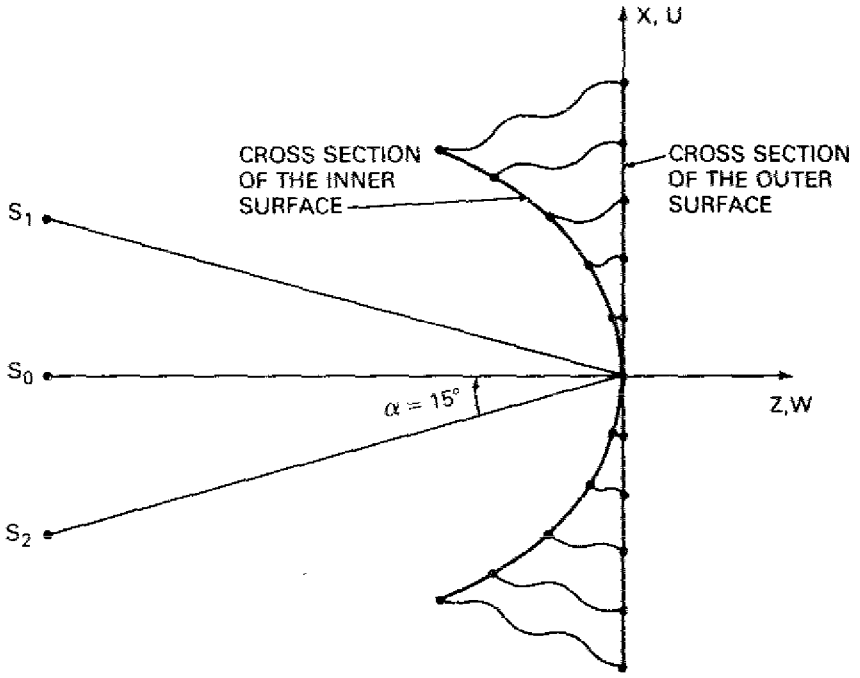

Fig. 7 — Cross section of a trifocal lens in XZ-plane, $\alpha = 15°$

APERTURE PHASE ERRORS: TRIFOCAL LENS

When a feed is displaced from the focal points to scan the beam to other angles, there will be some phase errors on the aperture. It is the purpose of this section to study these errors for trifocal lens. Let R be an arbitrary feed position on the feed line (a line passing through the focal points) such that the main beam direction is at an angle θ to the Z-axis, as shown in Fig. 6. Similar to a bifocal lens, if the feed location is confined to the feed line, the aperture phase errors are independent of the coordinate V and depend only on U and θ. Therefore, to know the aperture phase errors, one needs to find only the phase errors on the aperture cross section in the UW-plane.

The coordinates of the feed point R are given by $(-F_o \tan\theta, 0, -F_o)$. The path length from feed point R to the phase front, for a general ray passing through the point $P(X, O, Z)$ is given by

$$L_p = \overline{RP} + L - U \sin\theta. \tag{32}$$

Similarly, the path length of the central ray, passing through the origin C, is given by

$$L_c = \overline{RC} + L_o \tag{33}$$

Therefore, the path length error is

$$\Delta L = L_p - L_c = \overline{RP} - \overline{RC} - U \sin\theta + L - L_o. \tag{34}$$

From Fig. 6, one can obtain values of $\overline{RP}$ and $\overline{RC}$ as

$$\overline{RP} = \sqrt{(X + F_o \tan\theta)^2 + (Z + F_o)^2} \tag{35}$$

and

$$\overline{RC} = F_o/\cos\theta. \tag{36}$$

Eliminating Z from (35) using (30), one obtains

$$\overline{RP} = \sqrt{(F_o/\cos\theta)^2 + 2F_o\,(L_o - L) + (L - L_o)^2 + 2\,X\,F_o \tan\theta}. \tag{37}$$

Substituting $\overline{RP}$ and $\overline{RC}$ values from (36) and (37) in (34) and expressing $L - L_o$ and X in terms of U using (31) and (28), it can be shown that the normalized path length error is given by

$$\frac{\Delta L}{F_o} = B - u \sin\theta - (1/\cos\theta) + \sqrt{(1/\cos\theta)^2 - 2\,B + B^2 + 2\,u \tan\theta\,(1 - B\cos\alpha)}, \tag{38}$$

where

$$u = U/F_o \text{ and } B = u^2 \cos\alpha \cos^2(\alpha/2).$$

Figure 8 shows normalized path length errors for trifocal lens as a function of aperture dimension u, for $\alpha = 15°$. It may be noted that, similar to bifocal lens, the maximum error occurs for $u = -0.5$ for any given scan angle when the aperture is limited to a range of $u = \pm 0.5$. However, the path length error at $u = 0.5$ has an opposite sign compared to that at $u = -0.5$. Therefore, the maximum phase excursion on the aperture is proportional to the difference of path length errors at $u = -0.5$ and $u = 0.5$. This total maximum path length error is plotted as a function of scan angle in Fig. 9. For scan angles less than α (15° in the example), the peak error occurred for a scan angle of about 9°. For scan angles greater than α, the error increases with the increase in scan angle. It may be noted from Fig. 9 that, for scan angles in the range of ±17°, path length errors are less than .0011, whereas the

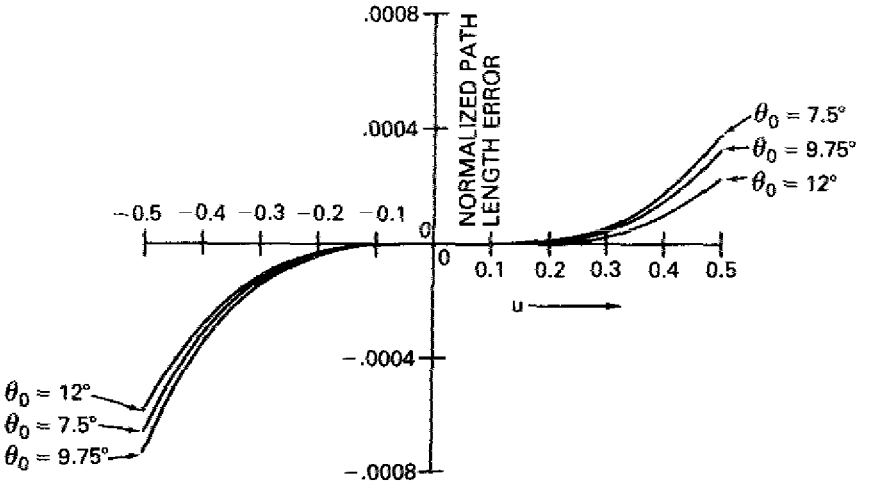

Fig. 8 — Path length errors in XZ-plane for a trifocal lens with $\alpha = 15°$

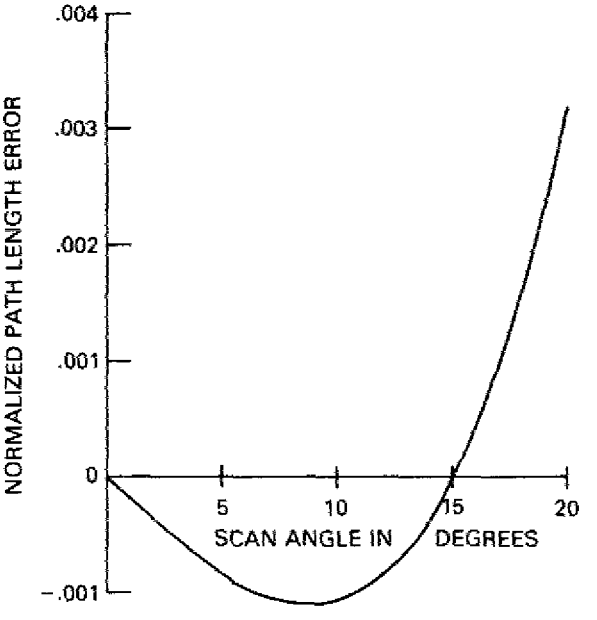

Fig. 9 — Path length error vs scan angle for a trifocal lens ($\alpha = 15°$)

single focus and bifocal lenses can be scanned to only $\pm 5°$ and $\pm 7°$ respectively. From Fig. 9, it was noted that the peak error occurs at a scan angle between 0 and α. This peak error increases with the increase in α. Figure 10 shows this relationship. This curve will be useful in choosing α for a specified peak phase (or path length) error. Once α is known, the scanning range, which is slightly larger than $\pm\alpha$, can be found for specified phase errors.

QUADRUFOCAL THREE DIMENSIONAL BOOTLACE LENS

Quadrufocal lens design differs from that of the trifocal case in that the outer surface of the lens is not constrained to a planar surface. This additional degree of freedom in design permits specification of four, rather than just three focal points. Lens symmetry dictates that those four focal points form two conjugate pairs. Figure 11 shows the lens cross section in XZ-plane. S_1, S_1', S_2 and S_2' are four

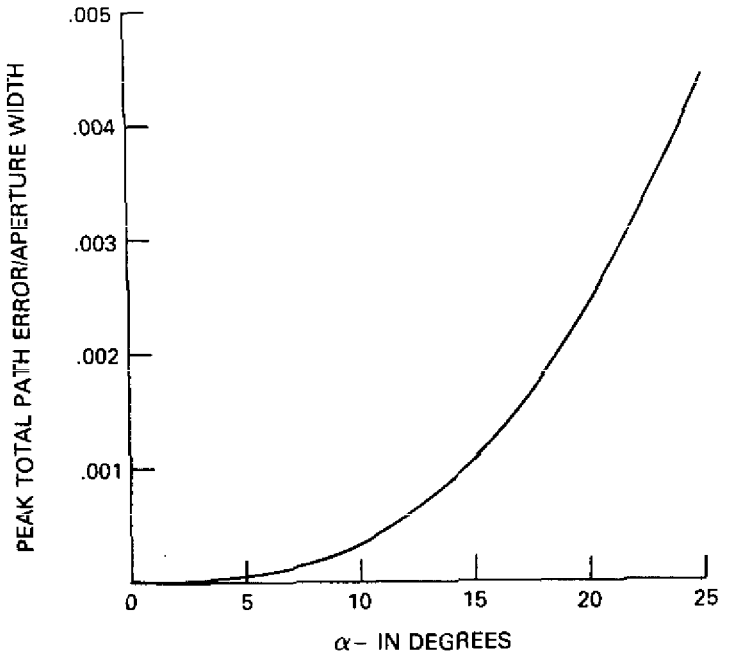

Fig. 10 — Peak total path length error vs α for a trifocal lens with $(F_0/D) = 1$

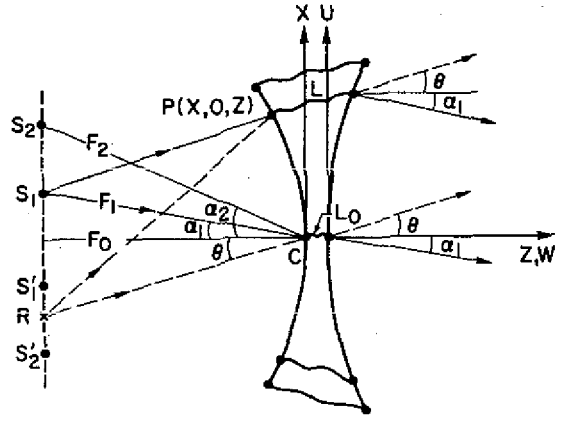

Fig. 11 — Quadrufocal lens geometry in XZ-plane

focal points for radiation at angles $-\alpha_1$, α_1, $-\alpha_2$, and α_2 to the W-axis respectively. The inner lens surface and locations of focal points are expressed in X, Y, and Z coordinates. The coordinates of the outer lens surface are expressed in U, V, and W. As discussed earlier with other lenses, the three dimensional inner surface of the lens can be obtained by rotating the lens cross section in XZ-plane about the feed line (the line on which the focal points are located). The outer surface of the lens will be shown to be a part of a circular cylinder.

Applying the path length equality from the focal point S_1, to the corresponding wave front yields

$$\overline{S_1P} + L - W\cos\alpha_1 + U\sin\alpha_1 = F_1 + L_o, \tag{39}$$

where

$$\overline{S_1P} = \sqrt{(X - F_1\sin\alpha_1)^2 + (Z + F_1\cos\alpha_1)^2}, \tag{40}$$

and

$$F_1 = \overline{S_1C}.$$

Similar to (39) and (40), the following relations can be obtained for focal points S_1', S_2, and S_2':

$$\overline{S_1'P} + L - W\cos\alpha_1 - U\sin\alpha_1 = F_1 + L_o, \tag{41}$$

$$\overline{S_1'P} = \sqrt{(X + F_1\sin\alpha_1)^2 + (Z + F_1\cos\alpha_1)^2} \tag{42}$$

$$\overline{S_2P} + L - W\cos\alpha_2 + U\sin\alpha_2 = F_2 + L_o, \tag{43}$$

$$\overline{S_2P} = \sqrt{(X - F_2\sin\alpha_2)^2 + (Z + F_2\cos\alpha_2)^2}, \tag{44}$$

$$\overline{S_2'P} + L - W\cos\alpha_2 - U\sin\alpha_2 = F_2 + L_o, \tag{45}$$

and

$$\overline{S_2'P} = \sqrt{(X + F_2\sin\alpha_2)^2 + (Z + F_2\cos\alpha_2)^2}, \tag{46}$$

where $F_2 = \overline{S_2C}$.

From (39) and (41) we obtain

$$\overline{S_1'P}^2 - \overline{S_1P}^2 = 4\,(F_1 + L_o - L + W\cos\alpha_1)\,U\sin\alpha_1. \tag{47}$$

Similarly, from (40) and (42) we have

$$\overline{S_1'P}^2 - \overline{S_1P}^2 = 4\,F_1\,X\sin\alpha_1. \tag{48}$$

Excluding the case of $\alpha_1 = 0$ (in that case S_1 and S_1' merge and becomes a special case having less than four focal points, which is already discussed), it is evident that right hand sides of (47) and (48) should be equal and the following relation is obtained:

$$X = (U/F_1)\,(F_1 + L_o - L + W\cos\alpha_1). \tag{49}$$

A similar result to (49) can be obtained by considering Eqs. (43) to (46), instead of (39) to (42), and is given below:

$$X = (U/F_2)\,(F_2 + L_o - L + W\cos\alpha_2). \tag{50}$$

Equating the right hand sides of (49) and (50), noting that $F_0 = F_1\cos\alpha_1 = F_2\cos\alpha_2$, the following relation can be obtained:

$$L - L_0 = W(\cos\alpha_1 + \cos\alpha_2). \tag{51}$$

Equation (51) can be used to find W, knowing $L - L_0$ or vice versa for given values of α_1 and α_2. A relationship between U and W or $L - L_0$ is required to finish the lens design. This is obtained in the following manner.

Substituting the value of $\overline{S_1P}$ form (39) in (40), squaring on both sides and eliminating X (but not X^2) using (49), one obtains

$$X^2 + Z^2 + 2Z\,F_1\cos\alpha_1 = (L - L_0)^2 + U^2\sin^2\alpha_1 + W^2\cos^2\alpha_1 - 2F_1(L - L_0) + 2F_1\,W\cos\alpha_1 - 2(L - L_0)\,W\cos\alpha_1. \tag{52}$$

Using the same procedure, an equation which is similar to (52) and corresponds to second conjugate pair of focal points can be obtained as

$$X^2 + Z^2 + 2\,Z\,F_2 \cos\alpha_2 = (L - L_0)^2 + U^2 \sin^2\alpha_2 + W^2 \cos^2\alpha_2 - 2\,F_2(L - L_0) + 2\,F_2\,W \cos\alpha_2 - 2(L - L_0)\,W \cos\alpha_2. \tag{53}$$

Knowing that $F_1 \cos\alpha_1 = F_2 \cos\alpha_2 = F_0$, it may be noted that left hand sides of (52) and (53) are equal. Equating right hand sides of (52) and (53), eliminating $L - L_0$ using (51) and simplifying, it can be shown that

$$U^2 + (W - R_0)^2 = R_0^2, \tag{54}$$

where

$$R_0 = F_0/\cos\alpha_1 \cos\alpha_2.$$

Equation (54) defines the cross section, in the UW-plane of the outer surface of the lens. The cross section is an arc of a circle of radius R_0 with a center at $W = R_0$. Therefore, the outer surface of the lens is a part of a circular cylinder.

An equation for the inner lens cross section is obtained using the following procedure. Eliminating $L - L_0$ and W in (52) using (51) and (54) one obtains

$$X^2 + Z^2 + 2\,Z\,F_0 = U^2(1 - \cos^2\alpha_1 - \cos^2\alpha_2). \tag{55}$$

It can be shown, using (49), (51), and (54), that U and X are related as

$$U^4 - U^2R_0^2 + X^2R_0^2 = 0, \tag{56}$$

or

$$U^2 = (R_0/2)\,(R_0 - \sqrt{(R_0^2 - 4X^2)}), \tag{57}$$

where R_0 is defined earlier in (54).

Substituting the value of U^2 from (57) in (55), one obtains the cross section in XZ-plane of the inner lens surface as

$$X^2 + (Z + F_0)^2 = F_0^2 + (R_0/2)\,(R_0 - \sqrt{(R_0^2 - 4X^2)})(1 - \cos^2\alpha_1 - \cos^2\alpha_2). \tag{58}$$

Therefore, the inner lens surface is given by

$$X^2 + Y^2 + (Z + F_0)^2 = F_0^2 + (R_0/2)\,(R_0 - \sqrt{(R_0^2 - 4X^2)})\,(1 - \cos^2\alpha_1 - \cos^2\alpha_2). \tag{59}$$

It is possible to eliminate the radical (square root) in (59) and obtain a fourth order equation for the inner surface of the lens. However, it will not be done here since (59) in its present form shows that for any given value of X, the inner surface is represented by a circular arc. For given values of F_0, α_1, α_2, and the element location U on the radiating surface, corresponding values of W and X can be found using (54) and (56). The corresponding value Z can be found from (58), knowing X, F_0, α_1 and α_2. Transmission line length $L - L_0$ can be found from (51), knowing W, α_1 and α_2. By assuming different values for U, complete inner surface cross section in the XZ-plane and the outer surface cross section in the UW-plane can be obtained. As an example, Fig. 12 shows the cross section of a quadrufocal lens with $\alpha_1 = 10°$ and $\alpha_2 = 25°$. The three dimensional inner surface of the lens can be obtained by rotating the cross section in XZ-plane about the line on which the focal points are located. The complete outer surface of the lens can be obtained by extending its UW-plane cross section towards the positive and negative V-axis. This completes the design procedure for the quadrufocal lens.

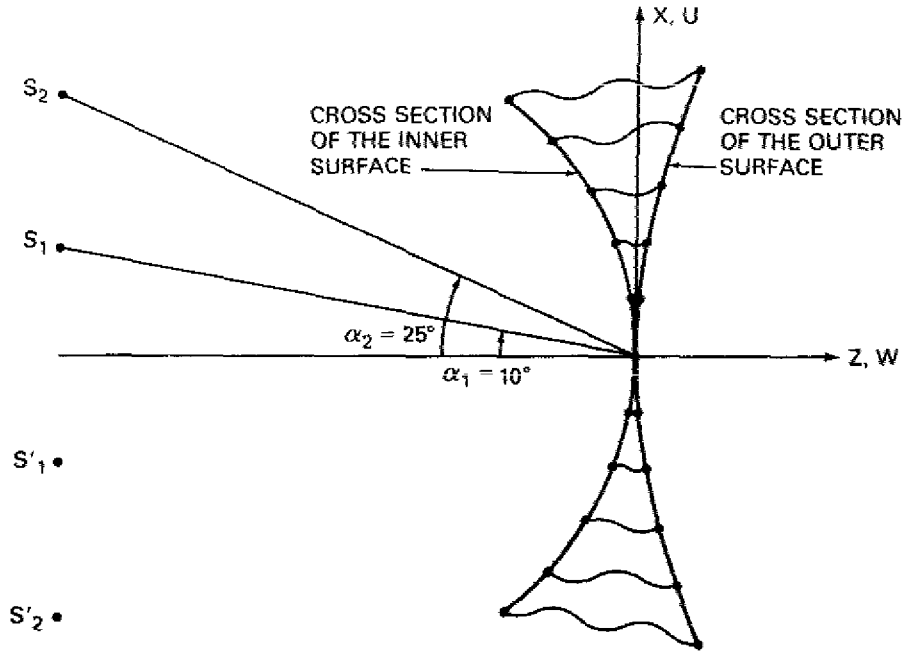

Fig. 12 — Cross section of a quadrufocal lens with $\alpha_1 = 10°$ and $\alpha_2 = 25°$

Requirements on the scanning range, allowable aperture phase errors, and the aperture size will determine what values should be chosen for design parameters F_0, α_1, and α_2. In this regard, the analysis on aperture phase errors, which is discussed in the next section, will be useful.

APERTURE PHASE ERRORS: QUADRUFOCAL LENS

Using a procedure quite similar to that used for bifocal and trifocal lenses, it can be shown that the normalized path-length error in the UW-plane, when the beam is scanned to an angle θ by placing a feed at R as in Fig. 11, is given by

$$\frac{\Delta L}{F_0} = d - u \sin\theta - w \cos\theta - (1/\cos\theta) + \sqrt{(1/\cos\theta)^2 + u^2(1 - \cos^2\alpha_1 - \cos^2\alpha_2) + 2x \tan\theta}, \tag{60}$$

where $d = \dfrac{L - L_0}{F_0}$, $u = \dfrac{U}{F_0}$, $w = \dfrac{W}{F_0}$ and $x = \dfrac{X}{F_0}$.

For a given value of U, corresponding values of W, $L - L_0$ and X can be found using (54), (51) and (56). Substituting these values in (60), the path length error can be found for specified values of F_0, α_1, α_2 and θ. Figure 13 shows normalized path length errors for the quadrufocal lens as a function of normalized aperture u, and for different scan angles when $\alpha_1 = 11°$ and $\alpha_2 = 25°$. It may be noted, similar to the bifocal lens, that the maximum error occurs for $u = -0.5$ for any given scan angle when the aperture width is limited to $u = \pm 0.5$. Figure 14 shows the maximum error as a function of positive scan angles for $\alpha_2 = 25°$ and for different values of α_1. For $\alpha_1 = 10°$, the peak phase error (for angles below α_2) occurs at an angle between α_1 and α_2. The peak value at zero degree scan angle is smaller than the peak value between α_1 and α_2. For $\alpha_1 = 11°$, those two peak values are approximately equal. For $\alpha_1 = 12°$, the peak value at zero degree scan angle is larger than the peak between α_1 and α_2. These observations point to a fact that there is an optimum value of α_1 for a given value of α_2 which makes those two peak phase errors equal and less than the peak error for any other value of α_1. Attempts to determine analytically this optimum value of α_1 for a given α_2 were not successful.

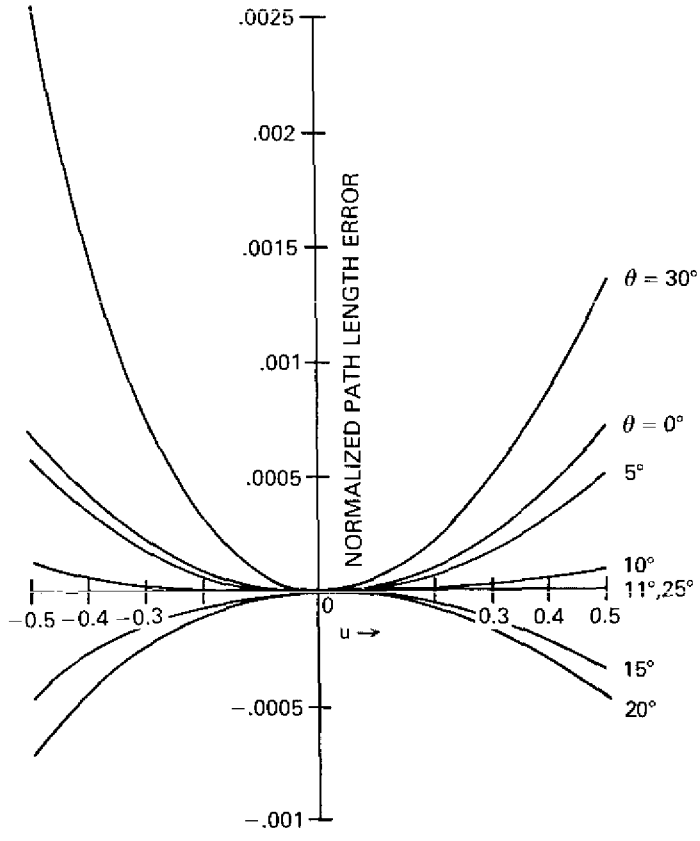

Fig. 13 — Path length errors in *XZ*-plane for a quadrufocal lens with $\alpha_1 = 11°$ and $\alpha_2 = 25°$

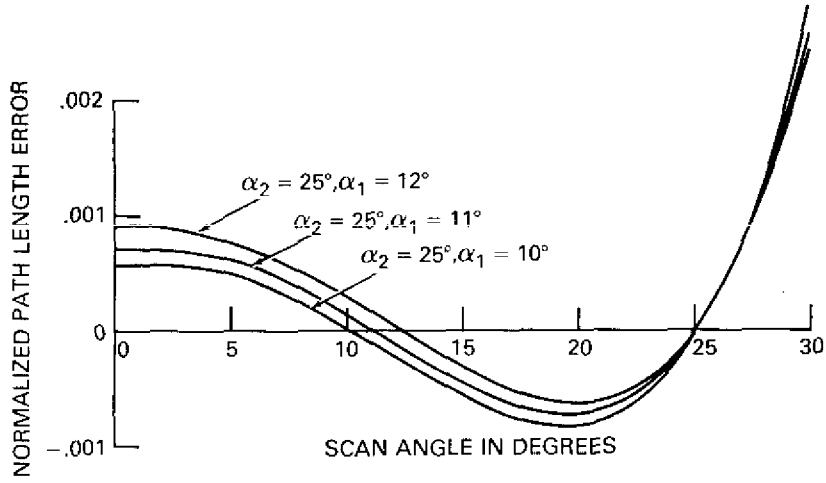

Fig. 14 — Path length error vs scan angle for quadrufocal lens

However, Mr. Paul Shelton suggested a method* of determining the approximate optimum value for α_1 and it is given by $\alpha_1 = \alpha_2$ (383/924). Then, the corresponding peak phase error can be obtained by substituting $\theta = 0$ in (60). Then, a curve, similar to Figs. 5 and 10, showing the peak error increasing with angle α_2, can be obtained as shown in Fig. 15. Therefore, for specified peak phase error, α_2 and the corresponding optimum value of α_1 can be found. Once α_2 is known, the scanning range, which is slightly larger than $\pm\alpha_2$ can be found using the method suggested by Mr. Paul Shelton. Using the approximate relation between the number of foci and maximum scan angle, as suggested by Mr. Shelton, and the results of Figs. 5, 10, and 15 one can obtain curves relating maximum scan angle for specified maximum path length error for all the lenses as shown in Fig. 15a. From that figure it is evident that for a given maximum path-length error, a lens with a larger number of focal points can be scanned to larger angles.

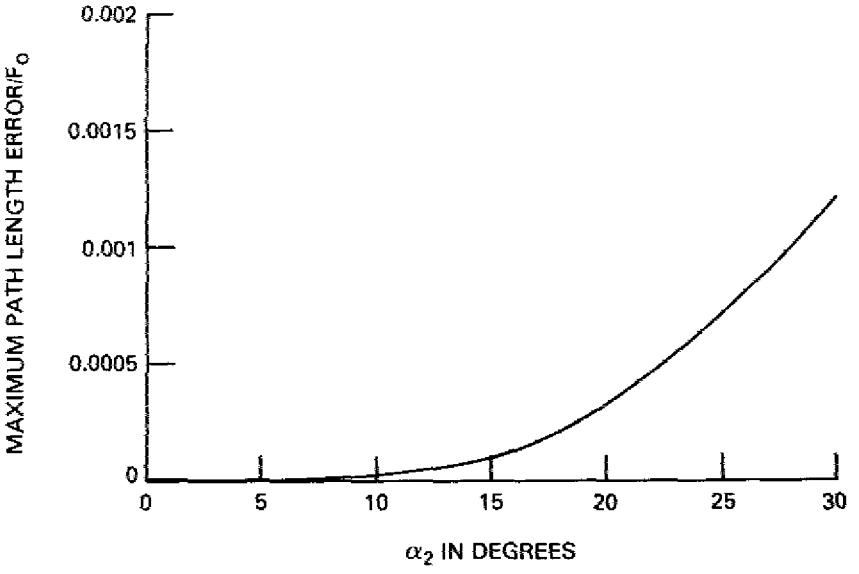

Fig. 15 — Maximum path length error vs α_2 for quadrufocal lens with $(F_0/D) = 1$

*Mr. Paul Shelton of NRL suggested the following analysis which can be used to find an approximate optimum value of α_1 for an assumed value of α_2 for quadrufocal lenses. His analysis can also be used in determining the maximum scan angle for a given α in bifocal and trifocal lenses and for a given α_2 in quadrufocal lenses.

"For the multifocal configuration, assuming that the phase error function is a polynomial in the scan angle or feed position, then the optimum polynomial is the Tchebycheff, $T_n(s) = \cos(n \cos^{-1} s)$, where n is the number of foci and s is the scan angle or feed position. Thus, the focus locations relative to maximum scan are given by $s = \cos(\pi/2n)$, $\cos(3\pi/2n)$, etc. For $n = 2$, $s = \pm 0.707$; for $n = 3$, $s = 0, \pm 0.866$; and for $n = 4$, $s = \pm 0.383, \pm 0.924$."

Using the above approximate analysis, the relations between maximum scan angle θ_{max} and feed positions (defined by the parameter α) are given below for lenses with different foci.

$\alpha = 0.707\,\theta_{max}$ for bifocal lens ($n = 2$)
$\alpha = 0.866\,\theta_{max}$ for trifocal lens ($n = 3$)
$\alpha_1 = 0.383\,\theta_{max}$ and
$\alpha_2 = 0.924\,\theta_{max}$ } for quadrufocal lens ($n = 4$).

The same Tchebycheff polynomial approximation can also be used in finding the angle θ_{peak} at which the path-length error is maximum by finding the θ value for which $T_n(\theta)$ is maximum. Knowing θ_{peak}, one can find maximum path-length errors for bifocal and trifocal lenses using Eqs. (18) and (38) for different values of α. It was verified that there is a very close agreement between the results obtained by this approximate method and those shown in Figs. 5 and 10.

So far, it is assumed that the scanning is accomplished by confining the feed to a straight line passing through the focal points. Only a limited investigation has been made on the scanning capability in the other planes. The results show that in the orthogonal plane (*VW*-plane) the scanning capability of multifocal lenses is limited and somewhat less than that of a single focus lens. Therefore, multifocal lenses are useful where the required scanning in one plane far exceeds that of the orthogonal plane [7].

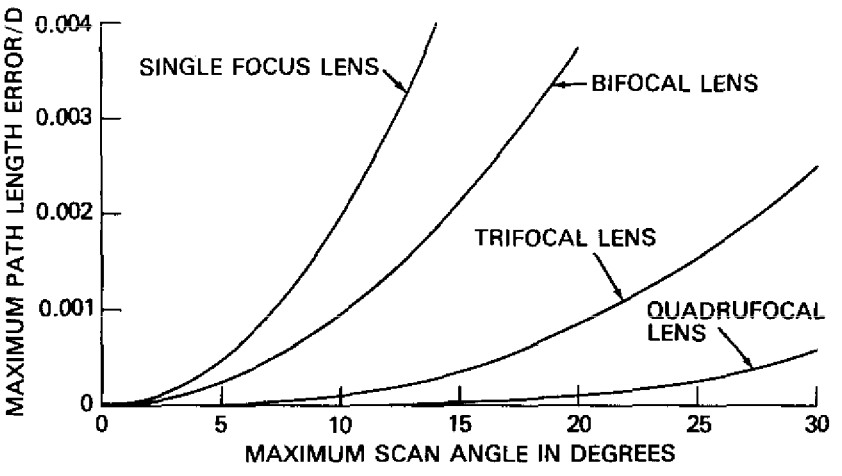

Fig. 15a — Maximum scan angle vs maximum path length error for different lenses

RADIATION PATTERNS

Computer simulation is used in obtaining radiation patterns for lenses discussed in this report. In addition to their geometries, effects of feed element pattern and pickup elements patterns are also included. Appendix A contains a detailed discussion on computer simulation. Radiation patterns were computed for lenses with radiating aperture of 60 λ by 60 λ and $(F_o/D) = 1$. The inter-element spacing is assumed to be λ/2. Figure 16 shows radiation patterns of a bifocal lens with $\alpha = 5°$. From earlier discussion on bifocal lens, it may be recalled that peak phase error occurs at zero scan angle and the scanning range is $\pm 1.4\ \alpha$. Therefore, patterns shown in Fig. 16 are the worst possible patterns, i.e., one at zero scan angle and the other at the scan limit. The corresponding peak error for $\alpha = 5°$ can be found from Fig. 5 and is given by .06 λ for 60 λ aperture width and $(F_o/D) = 1$. For a 10 dB amplitude taper on the aperture, one would expect the sidelobes to be about 21 dB below the mainlobe peak, if there are no phase errors. With the above stated errors, which are quite small, it may be seen from Fig. 16 that their effect on the sidelobes is negligible. Figure 17 shows two worst patterns in the scan range corresponding to $\alpha = 7.5°$. The corresponding peak error, from Fig. 5, is .228 λ (.0038 × 60λ). This error is not negligible and its effect on the radiation patterns can be seen from Fig. 17, i.e., shoulder formation.

Figure 18 shows radiation patterns for a trifocal lens with $\alpha = 18°$. The feed element pattern is chosen such that the aperture edges have a 10 dB amplitude taper when the feed is located on the axis (zero degree scan). From the earlier discussion on trifocal lenses it may be noted that there are no phase errors for the on axis beam and for the off axis beam at the angle α (18° in the example). As is noted from Fig. 18, the sidelobes are down by 21 dB for the on axis beam which is what one expects for a 10 dB amplitude taper. However, the sidelobes are higher for the 18° off axis beam. This is due to the decrease in amplitude taper on the aperture, when the feed is moved to produce off-axis beams. Therefore, the sidelobes can only be reduced by increasing the feed size for off-axis beams. For $\alpha = 18°$, the peak phase error for trifocal lenses may be obtained from Fig. 10 and is given by 0.1032 λ (0.00172 × 60λ), which occurs for a scan angle of about 11°. The effect of phase errors can be seen from patterns at scan angles of 11° and 15°. Sidelobes are unsymmetrical, being higher on one side and

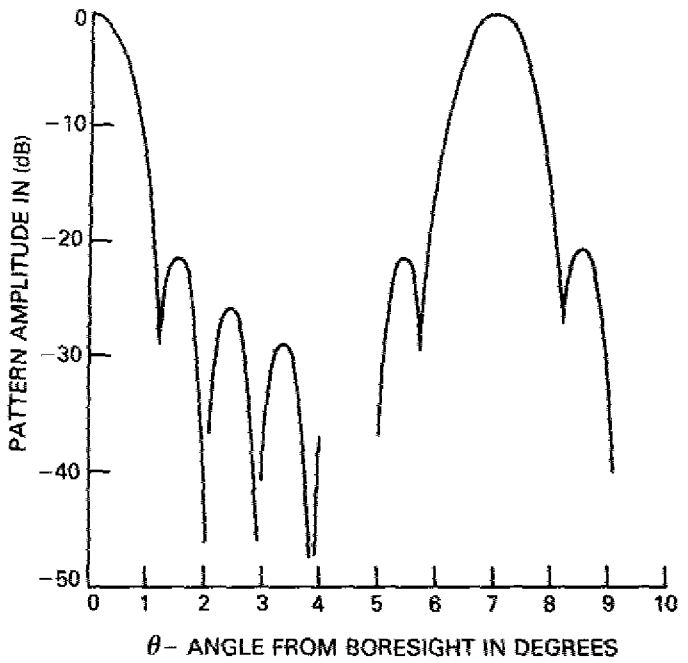

Fig. 16 — Scan plane patterns of bifocal lens with $\alpha = 5°$

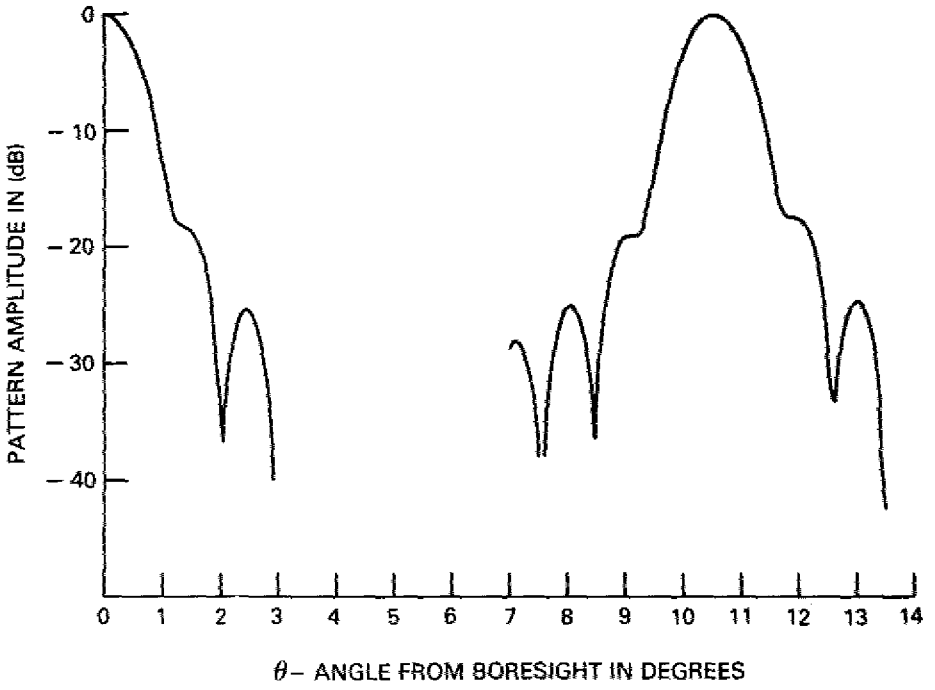

Fig. 17 — Scan plane patterns of bifocal lens with $\alpha = 7.5°$

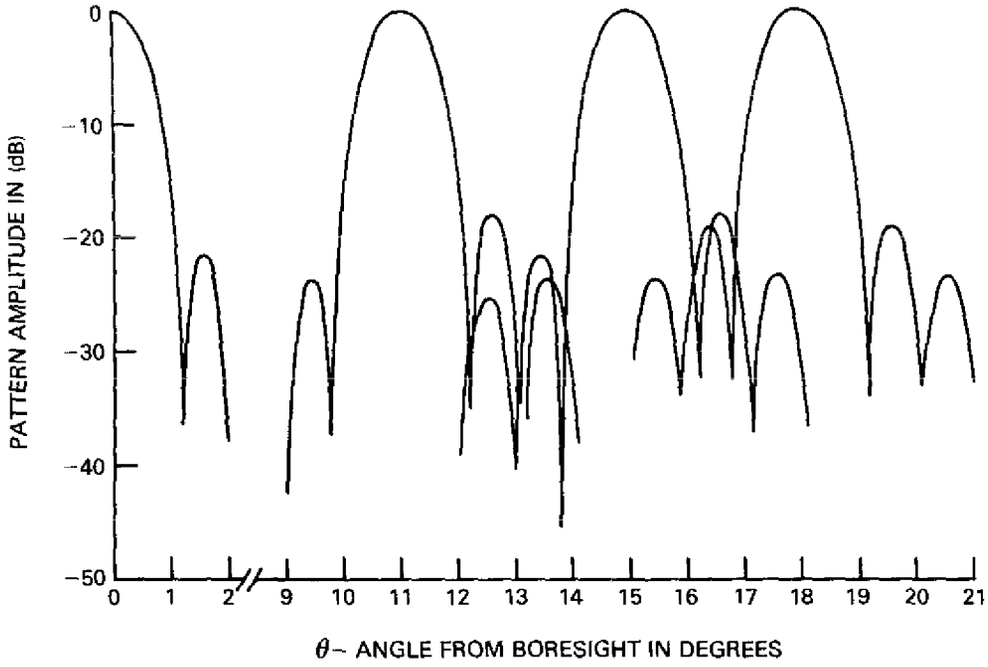

Fig. 18 — Scan plane patterns of trifocal lens with $\alpha = 18°$

lower on the other. Change in amplitude taper may also have some effect on the sidelobes. The value of $\alpha = 18°$ was purposely chosen to see the effects of phase errors. By choosing a smaller value for α (say 15°) the effect of phase errors can be reduced. However, it may be seen that the scanning range of a trifocal lens is at least twice as much as that of a bifocal lens.

Figure 19 shows the pattern of a trifocal lens in the orthogonal plane (ϕ-plane) when the beam is scanned to 11° in θ-plane. The pattern is symmetric and sidelobes are much lower compared to those in the scan plane.

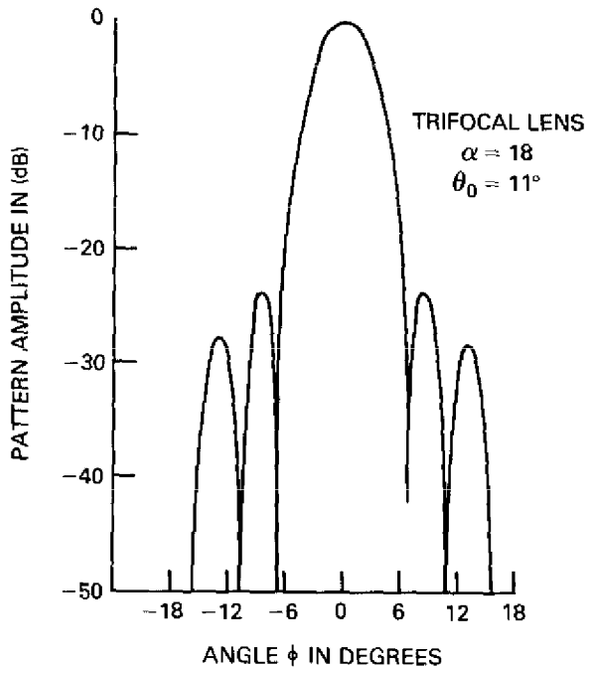

Fig. 19 — ϕ-plane pattern

Figure 20 shows two scan plane patterns of a quadrufocal lens (with $\alpha_1 = 11°$ and $\alpha_2 = 25°$), one on boresight and the other at 20° off axis. As can be seen from Fig. 14, the peak error on the aperture for these beams is 0.042 λ (0.007 × 60λ). Since this is a small error, it has negligible effect, as may be seen from the on-axis beam. For other beams in ± 27° range, peak aperture errors are smaller. The feed pattern used in computing these patterns is such that the on-axis beam has a 10 dB amplitude taper. However, using the same feed for off-axis beam gives slightly asymmetric amplitude distribution with less than 10 dB taper. This is the reason for sidelobes being higher for off-axis beam compared to on-axis beam. This indicates that a larger feed should be used for larger scan angles to obtain the same amplitude taper. Figure 21 shows patterns at 20° and 27° off-axis when feed patterns are chosen to obtain a 10 dB taper. Sidelobes are at −20 dB level, instead of −21 dB one would expect for a 10 dB amplitude taper.

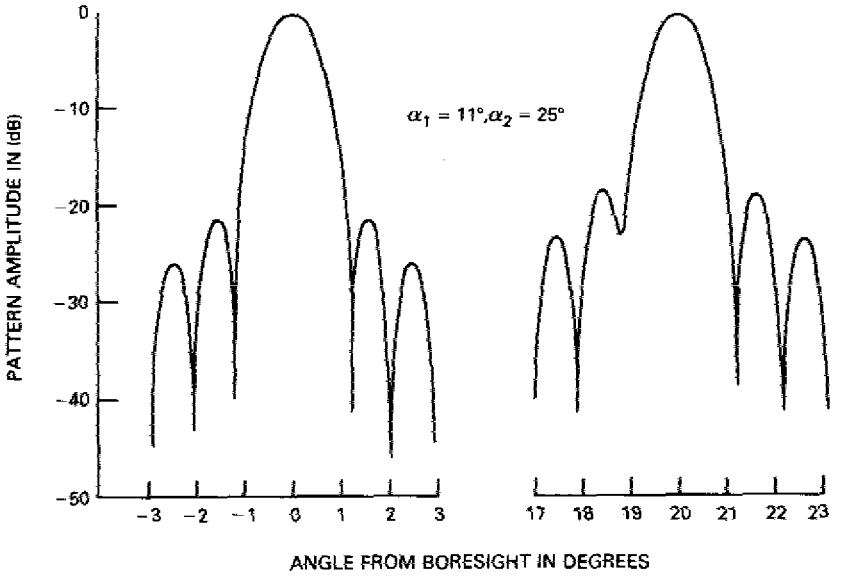

Fig. 20 — Scan plane patterns of quadrufocal lens with feed pattern independent of scan angle

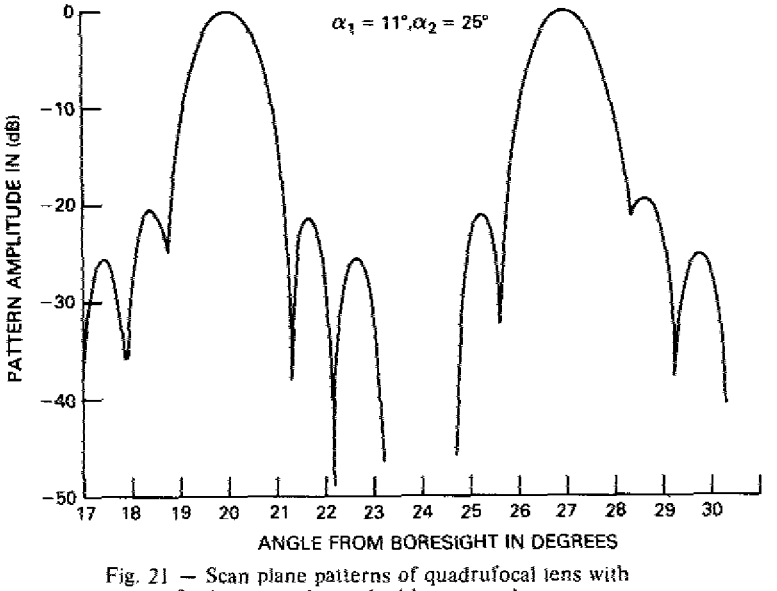

Fig. 21 — Scan plane patterns of quadrufocal lens with feed pattern changed with scan angle

CONCLUSIONS

Three dimensional bootlace lenses having two, three and four perfect focal points are proposed. Design equations are obtained for inner (pickup) and outer (radiating) surfaces for all three lenses. Aperture phase errors are analyzed when a feed is moved to scan the beam to different angles in a scan plane. The results of the analysis showed that the scanning capability of a lens increased with the increase in number of focal points. Computer simulation of radiation patterns are also presented for all three lenses. These results also show that a lens with a higher number of focal points can be scanned to larger angles. Our limited investigation also showed that the scanning capability of multifocal lenses is limited in the orthogonal plane and somewhat less than that of a single focus lens. Therefore, multifocal lenses are useful where the required scanning in one plane far exceeds that of the orthogonal plane.

REFERENCES

1. W. Rotman and R.F. Turner, "Wide-Angle Microwave Lens for Line Source Applications," IEEE Trans. on Antennas and Propagation, Vol. 11, No. 6, pp. 623-632, Nov. 1963.

2. M.L. Kales and R.M. Brown, "Design considerations for Two-Dimensional Symmetric Bootlace Lenses," IEEE Transactions on Antennas and Propagation," Vol. 13, No. 4, pp. 521-528, July 1965.

3. J.H. Provencher, "A Survey of Circular Symmetric Arrays," in "*Phased Array Antennas*," Edited by A.A. Oliner and G.H. Knittel, Artech House, Dedham, Mass., 1970.

4. J. Ruze, "Wide-Angle Metal-Plate Optics," Proc. IRE, Vol. 38, pp. 53-59, Jan. 1950.

5. A.R. Dion and L.J. Ricardi, "A Variable-Coverage Satellite Antenna System," Proc. IEEE, Vol. 59, pp. 252-262, Feb. 1971.

6. W.T. Patton, "Limited Scan Arrays," in "*Phased Array Antennas*," Edited by A.A. Oliner and G.H. Knittel, Artech House, Dedham, Mass., 1970.

7. G. Hyde, R.W. Kreutel, and L.V. Smith, "The Unattended Earth Terminal Multiple-Beam Torus Antenna," COMSAT Technical Review, Vol. 4, No. 2, pp. 231-262, Fall 1974.

Appendix
COMPUTATION OF RADIATION PATTERNS

As discussed in the text, let the radiating surface be specified in U, V, W coordinates. Since the cross section of the radiating surface is independent of the coordinate V, an element position on a radiating surface can be expressed as $(U_m,\ V_n,\ W_m)$, where m takes on values from 1 to M and n takes on values from 1 to N. Therefore, there are a total of MN elements. Then, the radiation pattern can be expressed as

$$E(\theta,\ \phi) = \sum_{m=1}^{M} \sum_{n=1}^{N} A_{mn} e^{j\frac{2\pi}{\lambda}(U_m \sin\theta\cos\phi + V_n \sin\theta\sin\phi + W_m\cos\theta + \xi_m)} \tag{A1}$$

Where θ, ϕ are the polar coordinates of a field point,

A_{mn} is the amplitude excitation of the element at $(U_m,\ V_n,\ W_m)$,

and

ξ_m is the phase excitation of the element at $(U_m,\ V_n,\ W_m)$ which is independent of V_n or n.

Results obtained from phase error analysis in the text can be used to find the appropriate expressions for ξ_m for all three lenses and will be given later. The procedure and formulation to find amplitude excitation A_{mn} is similar for all three lenses and is discussed below.

Figure A1 shows the geometry used in determining A_{mn}. Let S be the feed position such that the main beam is directed at an angle θ_0 to the W axis. The position of an element at P on the pickup surface is represented by $(X_{mn},\ Y_{mn},\ Z_{mn})$, and is connected by transmission line to a corresponding element $P_0\ (U_m,\ V_n,\ W_m)$ on the radiating surface. It is assumed that the feed element is tilted such that its pattern maximum is in the direction of SQ. Similarly, the pickup element is placed such that its pattern maximum is in the direction of PG. It is now evident that A_{mn} depends on the feed pattern, pickup element pattern, angle δ_{mn}, angle θ_{mn} and the distance $\overline{SP}$. Therefore, A_{mn} may be expressed as

$$A_{mn} = K^f_{mn}\ K^P_{mn}\ K^d_{mn}, \tag{A2}$$

where K^f_{mn} is feed element pattern factor,

K^p_{mn} is pickup element pattern factor,

and K^d_{mn} is the distance difference factor.

For computational purposes, the feed element pattern is assumed as a power of a cosine function and is given by

$$K^f_{mn} = \cos^{N_o}(\delta_{mn}), \tag{A3}$$

where N_o is an arbitrary constant to be chosen to give proper amplitude taper. The pickup element pattern is assumed to be of the form

$$K^p_{mn} = \frac{\sin\left\{\frac{\pi B}{\lambda}\sin\theta_{mn}\right\}}{\left\{\frac{\pi B}{\lambda}\sin\theta_{mn}\right\}}. \tag{A4}$$

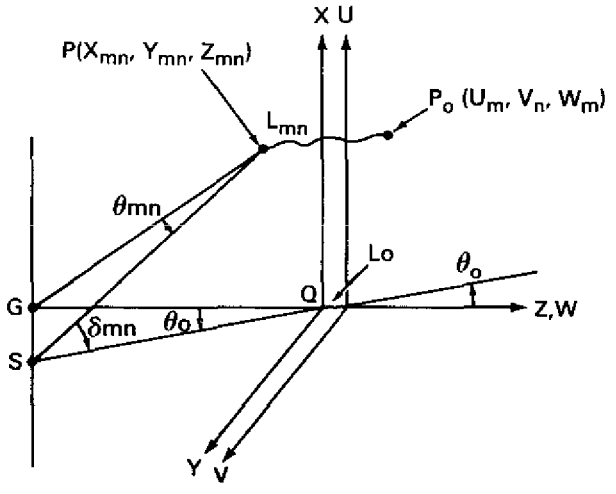

Fig. A1 — Geometry used in determining the amplitude excitation A_{mn}

For the results presented in the text, B is taken as $\frac{\lambda}{2}$.

The distance difference factor is given by (see Fig. A1)

$$K_{mn}^{d} = \frac{\overline{SQ}}{\overline{SP}} = \frac{F_o}{\cos\theta_o} \frac{1}{\sqrt{(X_{mn} + F_o \tan\theta_o)^2 + Y_{mn}^2 + (Z_{mn} + F_o)^2}} \tag{A5}$$

To use Eqs. (A3) and (A4) one needs to know δ_{mn} and θ_{mn}. Referring to Fig. A1 one can show that

$$\cos(\delta_{mn}) = \alpha_{sq}\,\alpha_{sp} + \gamma_{sq}\,\gamma_{sp}, \tag{A6}$$

and

$$\cos(\theta_{mn}) = \alpha_{ps}\,\alpha_{pg} + \beta_{ps}\,\beta_{pg} + \gamma_{ps}\,\gamma_{pg}, \tag{A7}$$

where

$$\alpha_{sp} = -\alpha_{ps} = (F_o \tan\theta_o + X_{mn})/d_{sp},$$
$$\beta_{ps} = -Y_{mn}/d_{sp},$$
$$\gamma_{sp} = -\gamma_{ps} = (F_o + Z_{mn})/d_{sp},$$
$$\alpha_{sq} = \sin\theta_o,$$
$$\gamma_{sq} = \cos\theta_o,$$
$$\alpha_{pg} = -X_{mn}/d_{gp},$$
$$\beta_{pg} = -Y_{mn}/d_{gp},$$
$$\gamma_{pg} = -(F_o + Z_{mn})/d_{gp},$$
$$d_{sq} = F_o/\cos\theta_o,$$
$$d_{sp} = \sqrt{(X_{mn} + F_o\cos\theta_o)^2 + Y_{mn}^2 + (Z_{mn} + F_o)^2},$$

and

$$d_{gp} = \sqrt{X_{mn}^2 + Y_{mn}^2 + (Z_{mn} + F_o)^2}.$$

The above formulation is common for all three lenses. They are used with the following relations obtained by using the information given in the text for individual lenses. In what follows, element coordinates U_m, V_n on the radiating aperture, F_o, aperture width D, α, α_1, and α_2 are assumed known or used as a variable parameter.

BIFOCAL LENS

$$W_m = 0$$

$$X_{mn} = U_m$$

$$Y_{mn} = V_n$$

$$Z_{mn} = -F_o + \sqrt{F_o^2 - X_{mn}^2 \cos^2\alpha - Y_{mn}^2}$$

$$\xi_m = (F_o/\cos\theta_o) - \sqrt{(F_o/\cos\theta_o)^2 + X_{mn}^2 \sin^2\alpha + 2\,X_{mn}\,F_o \tan\theta_o}.$$

TRIFOCAL LENS

$$W_m = 0$$

$$X_{mn} = U_m \left[1 - (U_m/F_o)^2 \cos^2\alpha \cos^2\frac{\alpha}{2}\right]$$

$$Y_{mn} = V_n$$

$$Z_{mn} = -F_o + \sqrt{[F_o - (U_m^2/F_o)\cos\alpha\cos^2(\alpha/2)]^2 - X_{mn}^2 - Y_{mn}^2}$$

$$\xi_m = (F_o/\cos\theta_o) - T - \sqrt{(F_o/\cos\theta_o)^2 - 2T\,F_o + T^2 + E}$$

where $T = U_m^2 \cos\alpha \cos^2(\alpha/2)/F_o$

and $E = 2\,U_m \tan\theta_o\,(F_o - T\cos\alpha)$.

QUADRUFOCAL LENS

$$X_{mn} = U_m \sqrt{1 - (U_m/F_o)^2 \cos^2\alpha_1 \cos^2\alpha_2}$$

$$W_m = F_o \left[1 - \frac{X_{mn}}{U_m}\right] / \cos\alpha_1 \cos\alpha_2$$

$$L_m = W_m\,(\cos\alpha_1 + \cos\alpha_2)$$

$$Y_{mn} = V_n$$

$$Z_{mn} = -F_o + \sqrt{F_o^2 + U_m^2\,(1 - \cos^2\alpha_1 - \cos^2\alpha_2) - X_{mn}^2 - Y_{mn}^2}$$

$$\xi_m = (F_o/\cos\theta_o) - L_m - \sqrt{(F_o/\cos\theta_o)^2 + U_m^2\,(1 - \cos^2\alpha_1 - \cos^2\alpha_2) + 2\,X_{mn}\,F_o \tan\theta_o}.$$